CR 86069

MC 67-264-R1

FAST RESPONSE SILICON PHOTOCONDUCTIVE DETECTORS

BY

MARK DOUMA

CONTRACT NO. NAS 12-523

PERIOD COVERED: JANUARY 15, 1967 - JUNE 15, 1967

FINAL REPORT

PREPARED FOR

NATIONAL AERONAUTICS AND SPACE ADMINISTRATION
ELECTRONICS RESEARCH CENTER

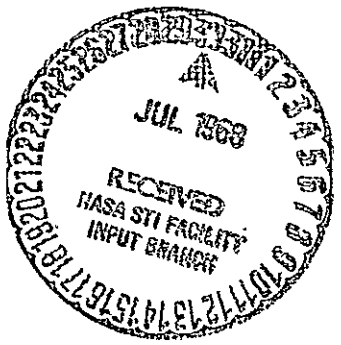

MITHRAS, INC.

AEROTHERMODYNAMICS – ELECTROMAGNETICS – QUANTUM PHYSICS

701 CONCORD AVENUE, CAMBRIDGE, MASS. 02138

MITHRAS, Inc.
701 Concord Avenue
Cambridge, Massachusetts
02138

MC 67-264-R1

FAST RESPONSE SILICON PHOTOCONDUCTIVE DETECTORS

by

Mark Douma

Contract No. NAS 12-523
Period Covered: January 15, 1967 - June 15, 1967

FINAL REPORT

Prepared for
National Aeronautics and Space Administration
Electronics Research Center

FOREWORD

This research was supported by the National Aeronautics and Space Administration Electronics Research Center under contract NAS 12-523. The technical guidance initially supplied by Mr. Louis Klieman and subsequently by Mr. Mark Gorstein is appreciated.

ABSTRACT

The response time of a silicon photoconductive detector in a circuit containing capacitance depends on the recombination time of the photo-generated carriers and the RC response time of the circuit. This RC response time is a function of the impedance of the detector. A linear model is developed which gives the response of the detector in the circuit to square light pulses of arbitrary duration. It is found that the maximum signal can occur at times much longer than the end of the pulse and that for short pulses the signal is proportional to the energy in the pulse. The model and the expected reduction in RC response time using low impedance detectors is verified experimentally. Results are used to determine the responsivity.

It is also found that the carrier recombination time in these detectors varies inversely with the field under high field conditions (greater than about 100 volts/cm). A minimum carrier response time of 30 nanoseconds is obtained. Possible mechanisms for this effect are discussed.

Current noise and Johnson noise are the only noise sources found measurable. The usual dependence of current noise on field, frequency, and dimensions is found to be approximately true. The detectivity as a function of light modulation frequency is computed for selected cases. A value of 5×10^{10} cm-cps$^{1/2}$/watt is found at 2 MHz.

ACKNOWLEDGEMENTS

The author would like to acknowledge the work of Mr. Russell Hubbard of MITHRAS who constructed the detectors used in this program. Also Dr. Arthur Linz of MITHRAS and the Massachusetts Institute of Technology, Crystal Physics Laboratory, who contributed immeasurably to the interpretation of the results.

TABLE OF CONTENTS

TABLE OF CONTENTS (CONT.)

LIST OF TABLES

LIST OF ILLUSTRATIONS

1. INTRODUCTION

In the past, near infrared (0.6 μ to 1.1μ) detectors have been dominated by silicon photovoltaic (PV) junction devices. Although a photoconductive (PC) detector is in principle simple, the purity of the silicon required to achieve an appreciable effect is so high that the usual procedures for passivation and contact formation are inadequate. Recently, MITHRAS has overcome these problems to the extent that photoconductive detectors are now comparable to the photovoltaic detectors in many areas. We will discuss briefly the PV devices in the Appendix.

Basically, a PC detector is just a light modulated conductance in series with a load resistor and connected to a bias voltage. The voltage across the load resistor is modulated by light of the appropriate wavelength (less than 1.1 μ.in silicon).

The main area in which PC detectors are not yet comparable to PV types is that where high light modulation frequencies are used - the response time is too long. This is not to say that PC detectors do not respond to short light pulses, but merely that the shape of the pulse is not reproduced by the signal. The response time of both PC and PV detectors is a function of two response times. One is the recombination time of the photogenerated carriers, and the other is the RC response time of the device and external circuitry. The recombination time of our usual PC detectors is on the order of 5 microseconds, but in addition the impedance is about 0.5 megohms, so that the RC effects can limit the response in some cases. The initial goal of this program was to construct and test detectors having interlaced finger electrodes to reduce impedance. However, during the tests of the low impedance detectors we found that the carrier recombination time was not constant, as is usually the case, but was reduced by the use of fields greater than about 100 volts/cm on the detectors. We devoted attention to this problem and obtained a minimum recombination time of about 30 nanoseconds.

Theories to handle the mechanisms of photoconductivity exist in the literature, but they are in most cases too general. In order to compare theory and experiment it is necessary to determine many parameters. Since practical silicon PC detectors are relatively new, we felt that at this stage a very simple model would be more useful for an

understanding of applications and for improving the characteristics of the device. Thus, in Section 2 we develop a quantitative linear model for the signal produced by a silicon PC detector in a circuit containing capacitance.

Section 3 describes the experiments performed to test the low impedance detectors and verify the model. A field-dependent recombination time is also described. The absolute responsivity is measured at 0.9 μ and compared with the model. In Section 4 we describe noise mechanisms and use measurements of the noise to compute D* as a function of frequency. Section 5 contains our conclusions and suggestions for improving the performance of PC detectors.

2. THEORY

2.1 The Change in Conductance of a Simple Bar Detector Upon Illumination

2.1.1 Neglecting Recombination

We will develop in this section an expression for the change in conductance of a simple bar detector upon illumination. We will arrive at the intuitively reasonable result that in the absence of recombination the fractional change in conductance is the number of absorbed photons divided by the total number of free carriers. This is not true in general, and the purpose of this section is to consider the assumptions which lead to such a result.

In semiconductors the bulk conductivity is given by the expression

$\sigma = neu_n + peu_p$ where

n = density of unbound electrons

p = density of unbound holes

u_n, u_p = respective mobilities (carrier velocities in a field of 1 v/cm)

e = magnitude of electronic charge

In an intrinsic semiconductor n = p, but usually there are impurities which increase one at the expense of the other (at fixed temperature np = constant in the absence of illumination), and it is extrinsic. Here we will be dealing with n-type material and we will assume that $n >> p$ and thus $\sigma = neu$. At fixed temperature and low enough fields (less than 1.5 Kv/cm) u_n is a constant, and the change in conductivity comes about through changes in n. This occurs when a photon with energy greater than the band gap (about 1.1 ev in silicon – equivalent to a wavelength of 1.13 microns) is absorbed by the sample. The effect is to create a non-equilibrium unbound electron and hole which increase the conductivity. (At high enough energies, more than one electron-hole pair can result, but we will always assume a yield of one). A great simplification results if we assume that the photo-generated holes have a very short lifetime and do not contribute to the increased conductivity. The above assumptions are possibly true only for low levels of illumination, but this is the most important case in practice.

Consider the simple bar detector of length ℓ, width w, and thickness d, as shown in Figure 2.1. In the figure G_{xy} is a differential element of conductance with respect to the indicated field of length ∂y, width ∂x, and thickness d. As shown in Figure 2.2 this can be broken into elements G_{xyz}. The change in conductance of G_{xy} upon illumination, ΔG_{xy}, is simply:

$$\Delta G_{xy} = \int_o^d \Delta G_{xyz}(z) \tag{2.1}$$

where ΔG_{xyz} is the change in G_{xyz} upon illumination.

If P_o monoenergetic photons/unit area are incident on the sample surface, then the number of photo-generated electrons at a depth z, assuming unit quantum yield, is

$$\Delta n(z) = Po\alpha\ e^{-\alpha z} \tag{2.2}$$

where α is the absorption coefficient at the particular wavelength. Since $\Delta G_{xyz} = \Delta neu_n\ \partial x \partial z/\partial y$ a[redacted]z

$$\Delta G_{xyz} = \Delta n\ eu_n \frac{\partial x}{\partial y}\ \partial z \tag{2.3}$$

In the case of the simple bar detector, the total conductance for uniform fields is

$$G = \left(\sum_y \sum_x \frac{1}{G_{xy}} \right)^{-1} \tag{2.4}$$

For low illumination levels, the change in conductance and fields will be small, hence the change in G is approximately

$$\Delta G = \sum_{x,y} \frac{G_o^2}{\left(\sum_x G_{oxy} \right)^2}\ \Delta G_{xy} \tag{2.5}$$

where G_o and G_{oxy} are the conductances in the absence of illumination. If we denote the unilluminated electron density by n_o, then, since $G_o = n_o eu_n wd/\ell$ and $G_{oxy} = n_o euwd/(\partial y)$, we have

$$\Delta G = \frac{eu_n(1 - e^{-\alpha d})}{\ell^2} \int_{x=o}^{w} \int_{y=o}^{\ell} Po(x,y)\ \partial x\ \partial y \tag{2.6}$$

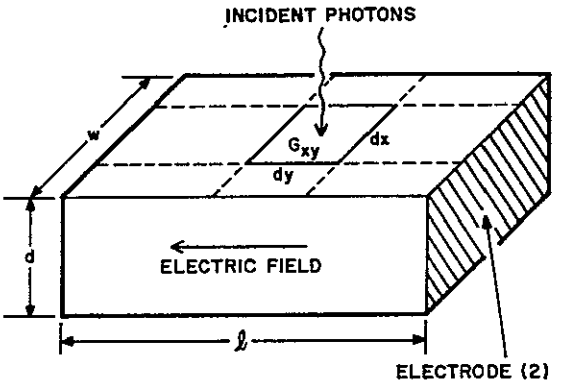

Figure 2.1 Simple Bar Cell Geometry

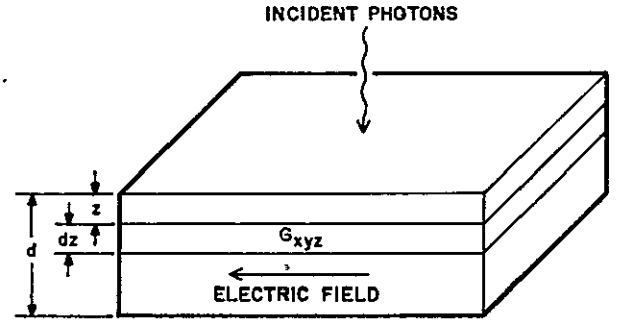

Figure 2.2 The Conductance Element G_{xy}

At this point we will make two simplifying assumptions. First, we will only consider uniform illumination, $P_o(x,y) = P_o$. Second, we will use a wavelength of 0.9 microns. For the cells used, the absorption coefficient has been found to be 500 cm^{-1} and the thickness about 0.01 cm. Thus the term $1 - \exp(-\alpha d)$ is approximately unity. We must, however, include a factor F, which is the transmission through the front surface after reflection losses. For normal incidence on a detector with a glass cover, this is given by

$$F = \frac{\left[1 - \left(\frac{n_g - 1}{n_g + 1}\right)^2\right]\left[1 - \left(\frac{n_{Si} - n_g}{n_{Si} + n_g}\right)^2\right]}{1 - \left(\frac{n_g - 1}{n_g + 1}\right)^2 \left(\frac{n_{Si} - n_g}{n_{Si} + n_g}\right)^2} \tag{2.7}$$

where n_g and n_{Si} are the indices of refraction of the glass and silicon, respectively. With $n_g = 1.5$ and $n_{Si} = 3.5$, F has the numerical value of 0.8. When the last three considerations are taken into account, Equation 2.6 simplifies to

$$\Delta G = F P_o e u_n \frac{w}{\ell} \tag{2.8}$$

The fractional change in conductance is

$$\frac{\Delta G}{G} = \frac{F P_o}{n_o d} = \frac{F P_o A}{n_o A d} \tag{2.9}$$

The last term on the right is just the total number of absorbed photons (equal to the number of photo-generated electrons) divided by the total number of free carriers in the unilluminated cell. This is the intuitive result referred to above.

2.1.2 Effects of Recombination

So far, other than the assumption that the holes recombine rapidly, we have not considered what happens to the electrons with time. In general, the photo-excited electrons may

1. recombine directly with a free hole,
2. become localized at trapping centers and get thermally reexcited before recombining,
3. recombine with a hole localized at a recombination center, or
4. recombine with a hole at a hole-injecting (positive) electrode.

The first case usually is not as probable as one of the latter three and has a time constant in the hundred microsecond region in silicon. The trapping case plays a role in stretching out the photo-response in PbS, CdS and CdSe detectors but is not predominant in silicon. Cases 3 and 4 are both important. We will look at case 4 experimentally in section 3.2.3. In this section we will be concerned with recombination centers with field independent microsecond time constants. Although not a great deal is known as to their nature, experiments with bulk samples indicate that the centers arise primarily at defects in the surface. This can add complexity to the problem, since we must consider the time for photo-generated electrons to diffuse to the surface. However, the assumption that the absorption coefficient is large implies that most of the excess carriers are generated near the surface and thus the diffusion time is short.

In the case of low light levels, a linear recombination equation holds:

$$\frac{\partial}{\partial t}\Delta n = \frac{-1}{\tau}\Delta n \tag{2.10}$$

where τ is the recombination time of the photo-generated electrons and may be a sum of several recombination times, viz.,

$$\tau^{-1} = \sum \frac{1}{\tau_i} \tag{2.11}$$

Since $\partial(\Delta G)/\partial t \propto \partial(\Delta n)/\partial t$ and assuming that the change in G and n is very small, we have

$$\frac{\partial}{\partial t}\frac{\Delta G(t)}{G_o} = \frac{F}{n_o d}\frac{\partial P_o}{\partial t} - \frac{1}{\tau}\frac{\Delta G(t)}{G_o} \tag{2.12}$$

At this point it will be convenient to consider the excitation in terms of watts instead of photons/sec. Thus,

$$\frac{\partial P_o}{\partial t} = KH(t) \tag{2.13}$$

where

H = number of watts/cm^2 incident on the sample

K = (wavelength in microns) x 5.13 x 10^{18} photons/sec/watt

With this change, Equation 2.12 can be rewritten,

$$\frac{\partial}{\partial t}\frac{\Delta G(t)}{G_o} + \frac{1}{\tau}\frac{\Delta G(t)}{G} = \frac{FK}{n_o d} H(t) \qquad (2.14)$$

For a constant light input, H_o, turned on at $t = 0$, this has the solution

$$\frac{\Delta G(t)}{G_o} = \frac{FKH_o\tau}{n_o d}(1 - e^{-t/\tau}) \qquad (2.15)$$

2.2 Signal Produced by a Photoconductor in a Circuit with Capacitance

2.2.1 General Solution

In this section we will use the results of section 2.1 for $\Delta G(t)/G$ to determine the signal obtained with a photoconductor in a circuit which includes both detector and stray capacitance. With the detector considered as a light modulated conductance, the equivalent circuit is as shown in Figure 2.3. A straightforward circuit analysis where ΔG is a function of time yields the following equation for S, the AC signal.

$$\frac{\partial S(t)}{\partial t} + \left[\frac{G_L + G_o + \Delta G(t)}{C_L + C_o}\right] S(t) = \frac{G_L}{G_L + G_o}\frac{E}{C_L + C_o}\Delta G(t) \qquad (2.16)$$

where

G_o = dark conductance of detector

C_o = capacitance of detector

G_L = conductance of series load

C_L = capacitance associated with load

E = constant bias voltage on detector and load in series

If $\Delta G(t)$ is known, the equation can be solved even though it is non-linear. A more illuminating approach is to develop a linear second order equation by making the usual assumption that $\Delta G(t) << $ either G_o or G_L. First we recast Equation 2.16 into the form

$$\frac{\partial S}{\partial t} + \frac{S}{\tau_e} = M(G_L/G_o)\frac{E}{\tau_e}\frac{\Delta G(t)}{G_o} \qquad (2.17)$$

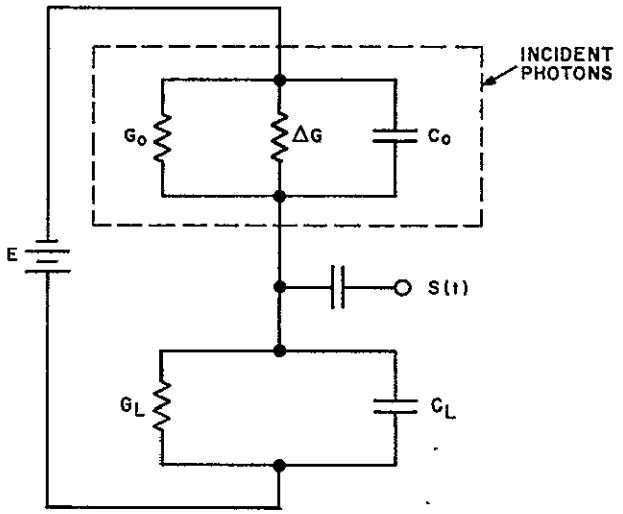

Figure 2.3 Equivalent Circuit for Detector Operation

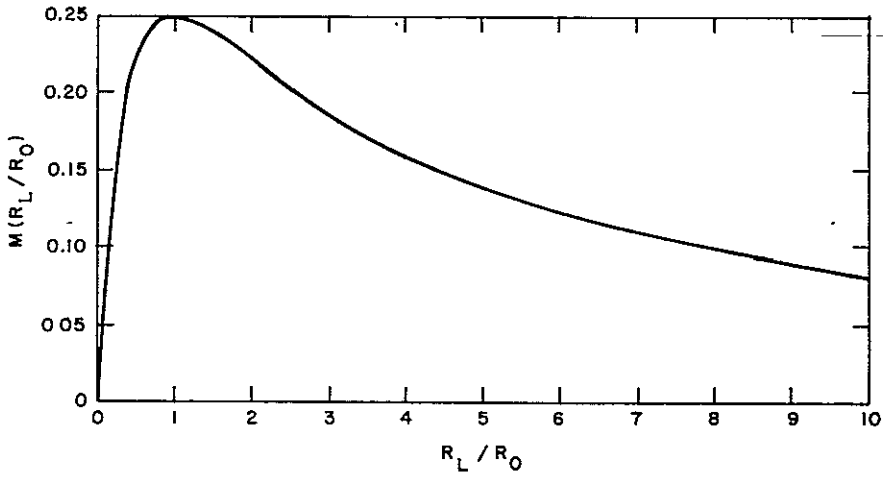

Figure 2.4 Load Mis-match Factor, $M(R_L/R_O)$, as a Function of R_L/R_O

where the electronic rise time is

$$\tau_e = \frac{C_L + C_o}{G_L + G_o} = \frac{R_L R_o}{(R_L + R_o)} (C_L + C_o) \tag{2.18}$$

and we shall define a load mis-match factor, M, as

$$M(G_L/G_o) = \frac{G_L G_o}{(G_L + G_o)^2} = \frac{R_L R_o}{(R_L + R_o)^2} \tag{2.19}$$

where R_L and R_o are the respective resistances. The function $M(R_L/R_o)$ is shown in Figure 2.4. It has a broad maximum at $R_L/R_o = 1$ and a value of 0.25 there.

Using the expression for $\Delta G(t)/G_o$, Equation 2.14, we have

$$\frac{\partial^2 S}{\partial t^2} + \left(\frac{1}{\tau_e} + \frac{1}{\tau}\right)\frac{\partial S}{\partial t} + \frac{S}{\tau_e \tau} = \frac{FMKE}{n_o d \tau_e} H(t) \tag{2.20}$$

which has the general solution

$$S(t) = \frac{FMKE\tau}{n_o d} \frac{1}{\tau - \tau_e} \cdot \int_o^t \left[e^{(q-t)/\tau} - e^{(q-t)/\tau_e}\right] H(q)\, dq \tag{2.21}$$

The above equations are analogous to a double low pass filter separated by an ideal isolation amplifier.

We shall restrict the remainder of this section to the response to a single square light pulse of duration T, i.e.

$H(t) = H_o$ for $0 \leq t \leq T$

$H(t) = 0$ otherwise.

The terms which do not depend on time may be collected into a voltage term

$$S_o = \frac{FMKE\tau}{n_o d} H_o \tag{2.22}$$

As will become apparent when we consider special cases, S_o is the maximum signal obtained with infinitely long pulses. It is the equilibrium photoconductive signal, and with a matched

load [$R_L = R_o$ so that $M(R_L/R_o)$ is maximized] it is a measure of sensitivity of the detector. The dependance on τ expresses the fact that there is a tradeoff of sensitivity for intrinsic detector speed.

In terms of S_o the solutions are

$$S(t < T) = S_o \frac{\tau(1 - e^{-t/\tau}) - \tau_e(1 - e^{-t/\tau_e})}{\tau - \tau_e} \tag{2.23}$$

and

$$S(t > T) = S_o \frac{\tau(1 - e^{-T/\tau})\, e^{-(t-T)/\tau} - \tau_e(1 - e^{-T/\tau_e})\, e^{-(t-T)/\tau_e}}{\tau - \tau_e} \tag{2.24}$$

For pulses of finite duration the maximum signal, S_m, is less than S_o and is given by

$$S_m = S_o\,(e^{T/\tau} - 1)^{\frac{\tau}{\tau - \tau_e}}\,(e^{T/\tau_e} - 1)^{\frac{\tau_e}{\tau_e - \tau}} \tag{2.25}$$

This occurs at a time, t_m, given by

$$t_m = T + \frac{\tau\tau_e}{\tau - \tau_e} \ell n \left[\frac{1 - e^{-T/\tau_e}}{1 - e^{-T/\tau}} \right] \tag{2.26}$$

Note that $t_m \geq T$ for all τ and τ_e.

2.2.2 Special Cases

Below we list special limiting cases.

Case 1: $\tau_e \to 0$. This occurs when either the parallel detector and load resistance or the capacitance is small. The response is determined by the detector. The solutions reduce to

$$S(t < T) = S_o(1 - e^{-t/\tau}) \tag{2.27}$$

$$S(t > T) = S_o(1 - e^{-T/\tau})\, e^{-(t-T)/\tau} \tag{2.28}$$

$$S_m = S_o(1 - e^{-T/\tau}) \tag{2.29}$$

$$t_m = T \tag{2.30}$$

Although analogous to a simple RC filter, the response time is determined by the recombination time only. However, the amplitude of the response to sinusoidally modulated light can be written

$$\frac{S_o}{\left(1 + (2\pi f\tau)^2\right)^{1/2}} \tag{2.31}$$

where f is the modulation frequency. This relation makes it possible to relate sinusoidal modulation and square pulse responses.

Case 1.1: $\tau_e \equiv 0$; $T \to 0$. This is a subcase of Case 1 and approaches the response to an impulse. The solutions are

$$S(t < T) = \frac{S_o t}{\tau} = \frac{ME}{n_o d} \; FKH_o t \tag{2.32}$$

$$S(t > T) = \frac{S_o T\, e^{-t/\tau}}{\tau} = \frac{ME}{n_o d} \; FKH_o T e^{-t/\tau} \tag{2.33}$$

$$S_m = \frac{S_o T}{\tau} = \frac{ME}{n_o d} FKH_o T \tag{2.34}$$

$$t_m = T \tag{2.35}$$

The signals are no longer a function of the recombination time. The response to an impulse (e.g., a Q-switched laser) is an almost instantaneous step with an exponential decay. The term $FKH_o T$ is just the number of photons absorbed from the pulse.

Case 2: $T \to 0$. This is the case for short pulses when τ and τ_e may be comparable.

$$S(t < T) = \frac{S_o t^2}{2\tau\tau_e} \tag{2.36}$$

$$S(t > T) = S_o T \; \frac{e^{-t/\tau} - e^{-t/\tau_e}}{\tau - \tau_e} \tag{2.37}$$

$$S_m = \frac{S_o T}{\tau} \left(\frac{\tau_e}{\tau}\right)^{\tau_e/(\tau - \tau_e)} \tag{2.38}$$

$$t_m = \frac{\tau\tau_e}{\tau - \tau_e} \ln \frac{\tau}{\tau_e} \tag{2.39}$$

This illustrates the effects of the circuit on the signal. The initial response is now quadratic instead of linear. The maximum signal in Equation 2.38 is less than in Equation 2.34 and t_m is now independent of pulse width.

Case 2.1: $T \to 0$; $\tau = \tau_e$. The magnitude of the effects of τ_e are illustrated by this case.

$$S(t < T) = \frac{S_o t^2}{2\tau^2} \tag{2.40}$$

$$S(t > T) = S_o \frac{Tt}{\tau^2} e^{-t/\tau} \tag{2.41}$$

$$S_m = S_o \frac{T}{\tau} e^{-1} = \frac{ME}{n_o d} FKH_o T e^{-1} \tag{2.42}$$

$$t_m = \tau \tag{2.43}$$

Comparing Equations 2.42 and 2.34 one can see that the reduction in response to an impulse is not very large even though the time, t_m, at which the maximum signal occurs, τ in this case, may be orders of magnitude later than the length of the pulse.

3. EXPERIMENTAL

3.1 Description of Detectors

3.1.1 Geometry

Five samples were used in all-three low impedance grid cells as shown in Figure 3.1 and two higher impedance simple bar cells in order to extend the range of analysis. Table 3. contains a compilation of geometrical data. In determining the effective length and width of the grid cells, they were considered as a set of narrow spaced bar cells in parallel. Thus the length is the distance between electrodes and the width is the number of elements times the length of each finger. The thickness of all cells was approximately 1.2×10^{-2} cm.

3.1.2 Impedance

The resistivity of the silicon was nominally 14,000 ohm-cm (equivalent to 6×10^{11} carriers/cc), but the samples were so thin that surface states contributed to the conductivity. The resistance was measured in the dark, and this was used to determine an effective concentration of carriers, n_o. These results are shown in Table 3.1, where it will be noted that n_o is higher than nominal for cell #1114-1, which had an 0.5 cm electrode spacing, and lower than nominal for close spaced electrodes. The latter case is due to a field concentration near the surface containing the electrodes when the electrode spacing approaches the thickness. Since we are interested in the product $1/n_o d$ we determined this from the equation

$$\frac{1}{n_o d} = e u_n Ro \frac{W}{\ell} \tag{3.1}$$

Although the mobility decreases at high fields, the measured resistance on these samples was almost linear with about a 5% increase in resistance at 1.5 Kv/cm. Using the usual value for electron mobility in silicon of 1.4×10^3 cm^2/volt-sec, we obtained the results for $1/n_o d$ shown in Table 3.1. An effective thickness is computed assuming the n_o of #1114-1 and is also shown.

The capacitive part of the impedance is quite small. Using the formula $C_o = \epsilon \epsilon_o wd/\ell$, cell #1120-2 should have the largest capacitance. For silicon, the low frequency ϵ is about 12, and thus, using the effective d, the capacitance is about 0.6 pf.

3.2 Response Times

In order to check the validity of Eq. 2.22 for the time-independent term, S_o, we need to determine the recombination time, τ. This section describes experiments to determine τ and check the validity of the solutions of section 2 for the response to square light pulses. We will also describe the field-dependent recombination time found in the close electrode-spaced cells.

3.2.1 Experimental Setup

Because of the difficulty in obtaining calibrated submicrosecond light sources, we used a different source for the absolute determination of S_o and the time-dependent terms. For the latter, the source used for generating square light pulses was a GaAs light emitting diode (Monsanto #MIE 200) driven by a Hewlett-Packard model 222A pulse generator which produces repetitive pulses of 30 nanoseconds to 5 milliseconds. The risetime of the generator was found to be less than 10 nanoseconds. Figure 3.2 is a picture of the 30 nanosecond pulse which has about a 25 nanosecond half-width. The diode has a peak output at 9000 A with a 400 A half-width. The rise-time of the diode was not measured but is specified as 5 nanoseconds. This was not noticeable in any of the measurements.

A totally enclosed metal box was used to contain the sample, load resistor and battery bias supply, and to reduce capacitance was mounted directly on an oscilloscope via a BNC connector. The oscilloscope used was a Tektronix Type 585 with Type 82 plug-in, which has a 10 nanosecond/cm sweep with a 4.5 nanosecond risetime. The total circuit capacitance of the plug-in and sample box was found to be 20 pf.

The diode was embedded in the end of a coaxial cable with a 50 ohm series resistor and fed into the sample box through a grounded metal pipe. There was some pickup of 500 MHz ringing at the beginning and end of the pulse which was not serious and could be used to determine the pulse length in some cases.

3.2.2 Effects of External Capacitance

In general, the response to square light pulses for all cells obeyed the equations developed in Section 2.2. In this section we will only illustrate the effects of external capacitance with results for cell #1114-1 and cell #1041-1.

In Section 2.2 we found that the response as a function of time was determined by the photoconductive response time, τ, and the electronic response time, τ_e. Experimentally, in order to vary τ_e we did not change the external capacitance but varied the load resistor, R_L. Two sets of data were taken for each cell. In the first set we used a matched load which yielded a τ_e comparable to τ. In the second set R_L was reduced to the point where τ_e was much less than τ. This reduces the signal through the dependance, $M(R_L/R_0)$; it is the motivation for developing low impedance detectors when external capacitance is present. The experiments consisted of illuminating the cells with square light pulses of constant amplitude and various durations, T. The signal was displayed on the oscilloscope and photographed.

For cell #1114-1 the first set used a matched load and a bias of 45 volts. Under these conditions, τ_e was 3.6 microseconds. The signals for pulse durations from 500 microseconds to 25 nanoseconds are shown in Figures 3.3, 3.4, and 3,5. One can see that as T decreases, the maximum signal, S_m, tends to occur at the constant time, t_m. Using Eq. 2.39 and $\tau = 5.75$ microseconds (the determination is discussed below), t_m should be 4.5 microseconds, which is approximately correct. In general, the response is given by the equations of Case 2 in Section 2.2.2.

For the second set, the same bias was used but the load resistance was reduced to 5.1 K ohms. This reduces τ_e to 0.1 microseconds and thus the response time is determined by the detector. The signals for pulse durations from 5 microseconds to 50 nanoseconds are shown in Figure 3.6 and Figure 3.7. One can see that Case 1 of Section 2.2.2 applies. The major effect is that very short pulses yield the simple exponential response of the detector.

The dependence of the maximum signal, S_m, on T was computed by using Eq. 2.25 for the first set and Eq. 2.29 for the second set. The results were normalized to the experimental value for an 0.3 microsecond pulse. The theoretical and experimental data are shown in Figure 3.8. The disagreement for long pulses probably occurs because the percentage change in conductance is about 30% in this region and a saturation effect occurs. This, of course, violates one of the assumptions in the development of the theory.

We will not consider cell #1041-1 in detail since results were similar. This cell had a shorter time constant (about 0.5 microseconds) and a lower impedance (35 K ohms) so that faster responses could be achieved. With a 50 K load ($\tau_e = 0.4$ microseconds) the

maximum time, t_m, is reduced by an order of magnitude. An example which illustrates Case 2.1 of section 2.2 is the response to a 25 nanosecond pulse shown in Figure 3.9. When the load is reduced to 510 ohms, so that $\tau_{e_2} = 10$ nanoseconds, response times illustrated in Figure 3.10 are obtained. Lastly, the t^2 dependence of Case 2, Eq. 2.36, is shown in Figure 3.11, again with a 510 ohm load.

3.2.3 Field Dependent Response Times

While checking the response time of the close-spaced electrode cells (numbers 1135-1, 1120-2 and 1135-2) it was found that the detector response time was reduced as the bias was increased. This is illustrated for sample #1135-2 in Figures 3.12, 3.13, 3.14, 3.15 and 3.16, where the response is shown as a function of voltage on the sample. In all except Figure 3.16 the measurements were made with a 1 K ohm load. In Figure 3.16 a 200 ohm load was used to reduce τ_e sufficiently. Similar results were obtained with sample # 1135-1 and are shown in Figures 3.17 and 3.18. These last two figures are difficult to interpret since the risetimes of the light source and oscilloscope begin to become important. Sample #1120-2 showed similar results also. Initially, an almost exact 1/E dependence on bias up to 2 Kv/cm was found for this sample, but this could not be obtained a second time. Increasing bias still reduced τ, but not exactly as 1/E. Further, at the same bias τ was less by a factor of 3 than it had been. The most probable reason is that the high fields and local heating changed the surface characteristics.

The response time, τ, at various field strengths is shown in Table 3.2 for all three samples. The carrier drift velocity, $(uE/\ell)\ (R_o/(R_L + R_o))$, and the transit time between electrodes, $(\ell^2/uE)\ \left((R_L + R_o)/R_o \right)$, are also listed. There are two simple models which might account for the field dependent recombination time. One is that electrons are recombining at a hole-injecting electrode. It can be seen that the response time (really the recombination time) is always longer than the transit time between electrodes. This could be explained by postulating that the mobility is reduced near the surface where the fields are concentrated. On the other hand, the surface recombination time is inversely proportional to a surface recombination velocity, which for low fields is on the order of a thousand cm/sec. The results do not rule out one or the other.

3.3 Determination of S_o and Responsivity

3.3.1 Experimental Setup

To experimentally determine S_o, we need a calibrated source and long duration light pulses ($T >> \tau$). For this a Barnes model 11-200-3 1000° C black body and a 620 Hz mechanical chopper were used. A calibrated Baird Atomic #B9 narrow-band filter with peak transmission at 9045 A and 91 A half-width was inserted between the source and sample. The energy falling on the sample was computed from the transmission of the filter and the theoretical black body characteristics by numerical integration.

The signal was amplified by a P. A. R. Model CR-4 low noise amplifier and the 620 Hz component determined with a Hewlett-Packard Model 302 A wave analyzer. (Use of a wave analyzer is restricted to cases where the response to light is linear; however, on sample #1114-1 this was true within a few percent over six orders of magnitude of light intensity. The range is determined on the upper end by the restriction that $\Delta G/G_o$ is small, and on the lower end by the noise.)

3.3.2 Results

The experiment performed was to determine the absolute value of S_o and check its dependence on bias, E. All five samples were placed in the same photon flux of 1.2×10^{-7} watts/cm^2, and S_o was measured as a function of E under matched load conditions. Note that the voltage on the sample is E/2. The results appear in Table 3.3.

The response is linear at low fields and approaches a constant as higher biases are used. This is what is expected if τ varies as 1/E, since S_o is proportional to $E\tau$. The effect is the most pronounced in cell #1135-1, which has the narrowest spacing. At high enough fields the response decreases. The decrease at 45 volts bias may be related to heating, since cells #1120-2 and #1135-2 have the lowest resistance.

Rather than computing S_o from Eq. 2.22 we will compute a related parameter, the responsivity, R. This is defined as the signal per watt incident on the cell, and hence

$$\mathcal{R} = \frac{S_o}{H_o A} = \frac{FMKE\tau}{mN_o dA} \qquad (3.2)$$

This is computed using values found previously and the results for 45 volts bias are shown in Table 3.4 along with the experimental values. Cell #1120-2 is not included, since

τ was not found at 45 volts. Experimentally it had a responsivity of 3.33×10^3 volts/watt there.

The results are not far out of line. Although this may be somewhat fortuitous, cell #1114-1 is a fairly simple case and should agree reasonably well. The widest divergence occurs for cell #1135-1. It could be that the recombination time is faster, and it is very probable that there are added complications due to the close spacing.

TABLE 3.1

SAMPLE SPECIFICATIONS

Sample #	1114-1	1135-1	1041-1	1120-2	1135-2
Type	Square	Narrow Bar	6 grid	19 grid	19 grid
Electrode spacing, (cm)	.5	.0075	.1	.012	.016
Width of active area (cm)	.5	.2	.4	.4	.4
Number of active bars	1	1	5	18	18
Equivalent width, w (cm)	.5	.2	2	7.2	7.2
Active area, w (cm^2)	.25	.0015	.2	.0864	.115
Resistance (K ohms)	360	110	35	3.7	11
Equivalent number of carriers/cc, $n_o \times 10^{-11}$	10.3	1.26	5.3	1.68	.75
Effective thickness (cm)	.012	.0015	.0062	.002	.00087
$(n_o d)^{-1} \times 10^{10}$	.81	6.6	1.6	5	11

TABLE 3.2

FIELD DEPENDENT RECOMBINATION TIME

Sample #	Voltage on Sample	Field (Kv/cm)	Response Time, (nsec)	Drift Velocity (cm/sec x 10^{-6})	Transit Time (nsec)
1120-2	.375	.03	865	.044	275
	.75	.062	500	.087	137
	1.5	.125	300	.175	68
	3	.25	200	.35	34
1135-1	6	.8	140	1.12	6.7
	12	1.6	100	2.24	3.35
	22.5	3.0	70	4.2	1.8
	45	6.0	30	8.4	.9
1135-2	1.5	.094	520	.13	122
	3	.188	430	.26	61
	6	.375	300	.52	30.5
	12	.750	230	1.04	15.2
	22.5	1.400	72	1.96	8.2

TABLE 3.3

S_o AS A FUNCTION OF BIAS

Sample # / Bias, E (volts)	1114-1	1041-1	1120-2	1135-1	1135-2
1.5	61 v	36 v	10.5 v	18 v	18.5 v
3	120	72	19	24	35
6	240	145	30.5	29	68
12	480	280	47	33	100
22.5	840	440	58.5	35	150
45	1700	690	50	36	140

TABLE 3.4

COMPARISON OF THEORETICAL AND EXPERIMENTAL RESPONSIVITIES AT 45 v BIAS

Sample #	Theoretical Responsivity	Experimental Responsivity
1114-1	7.5×10^4 volts/watt	5.7×10^4 volts/watt
1041-1	1.6×10^4	2.3×10^4
1135-1	1.3×10^6	2.0×10^5
1135-2	2.8×10^4	1.0×10^4

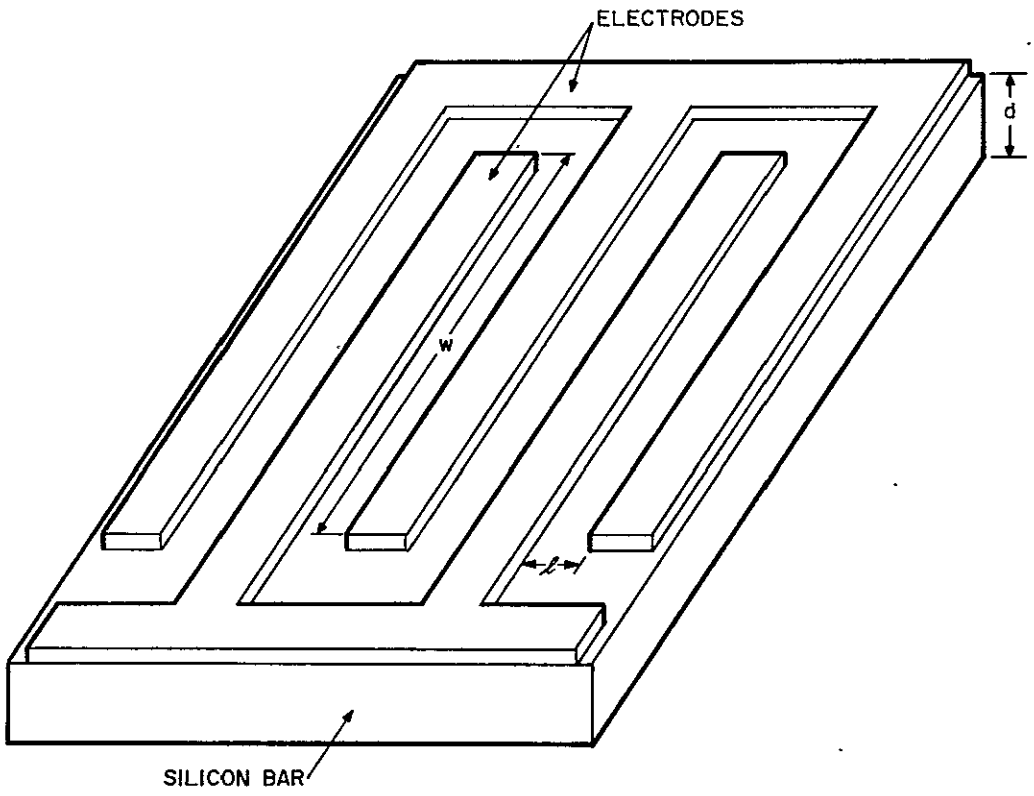

Figure 3.1 Grid Cell Geometry

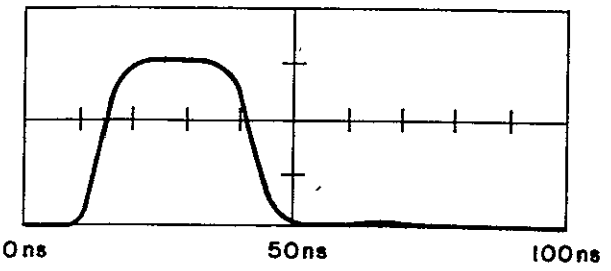

Figure 3.2 Square Wave Pulse Generator Output on 30 ns Setting

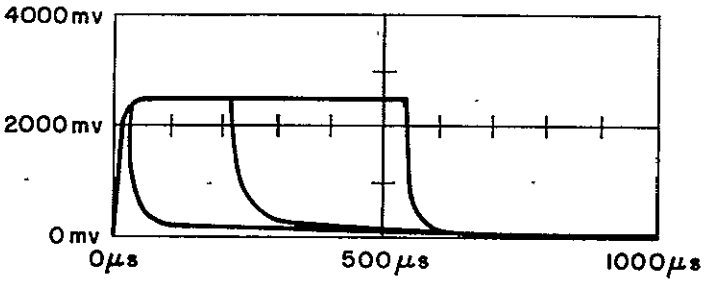

Figure 3.3 Response of Cell #1114-1 for T (right to left) = 500 μs, 200 μs, 50 μs

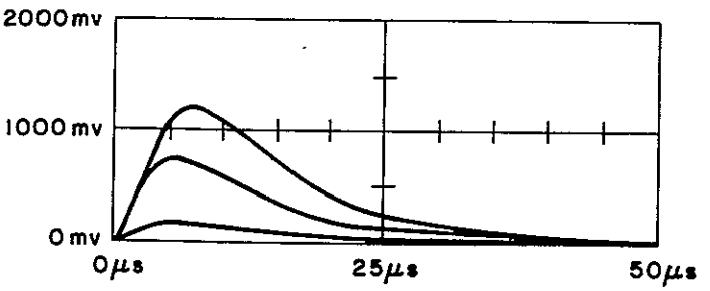

Figure 3.4 Response of Cell #1114-1 for T (top to bottom) = 5 μs, 2.5 μs, 0.5 μs

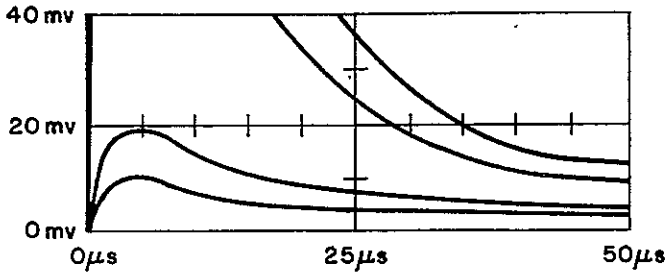

Figure 3.5 Response of Cell #1114-1 for T (top to bottom) = 500 ns, 250 ns, 50 ns, 25 ns

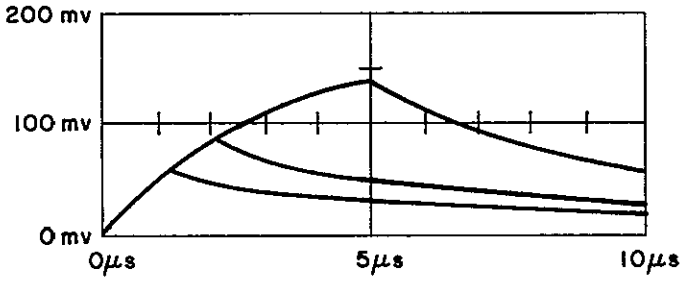

Figure 3.6 Response of Cell #1114-1 for T (right to left) = 5 μs, 2 μs, 1 μs

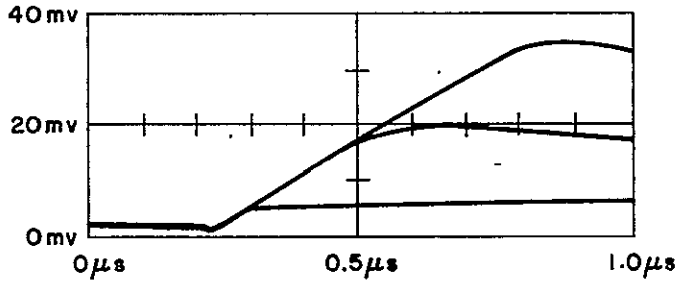

Figure 3.7 Response of Cell #1114-1 for T (top to bottom) = 500 ns, 250 ns, 50 ns

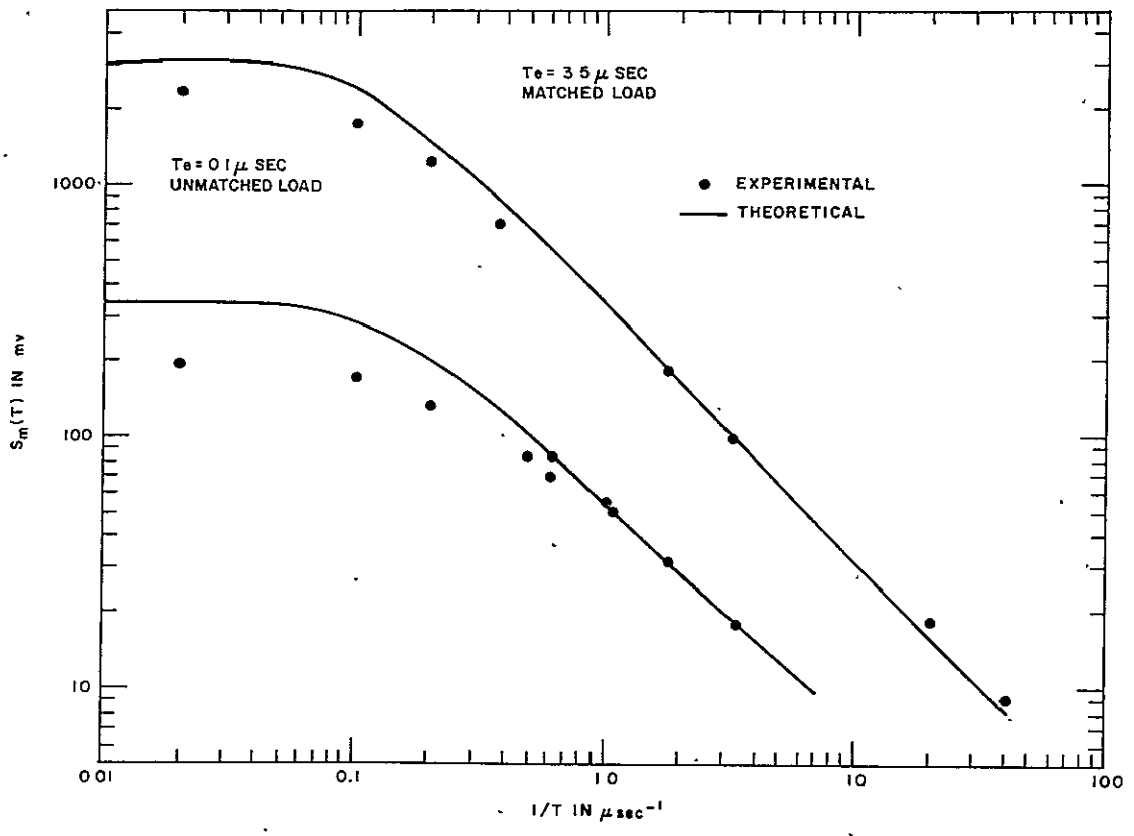

Figure 3.8 $S_m(T)$ vs. $1/T$ for Cell #1114-1

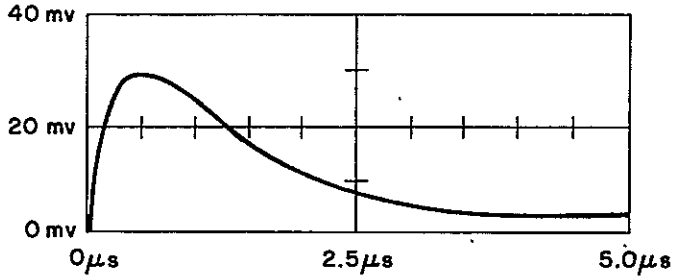

Figure 3.9 Response of Cell #1041-1 for T = 25 ns

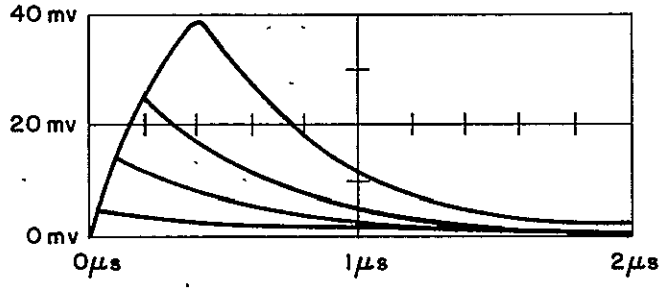

Figure 3.10 Response of Cell #1041-1 for T (top to bottom) = 400 ns, 200 ns, 100 ns, 25 ns

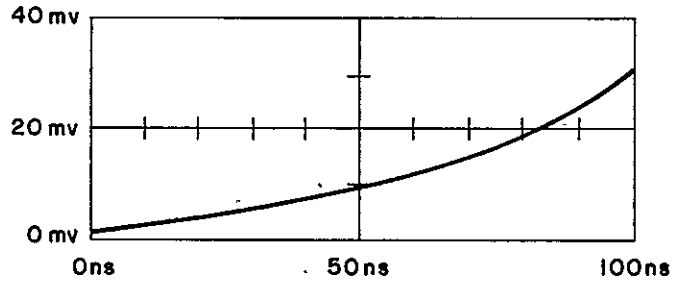

Figure 3.11 Initial t^2 Dependence of Response for Cell #1041-1. T > 100 ns

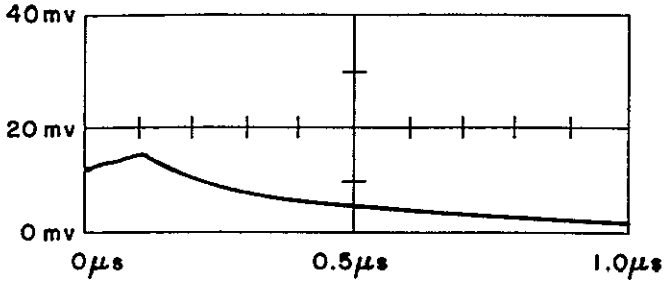

Figure 3.12 Photoconductive Decay for Cell #1135-2. E = 1.5 volts

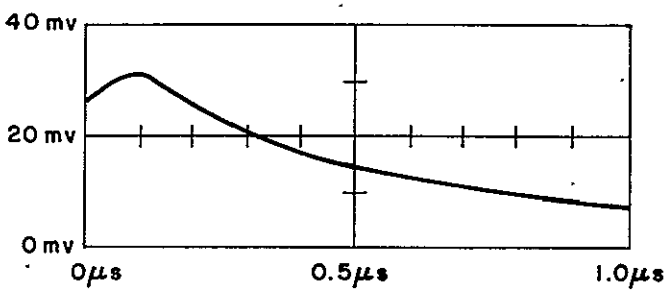

Figure 3.13 Photoconductive Decay for Cell #1135-2. E = 3 volts

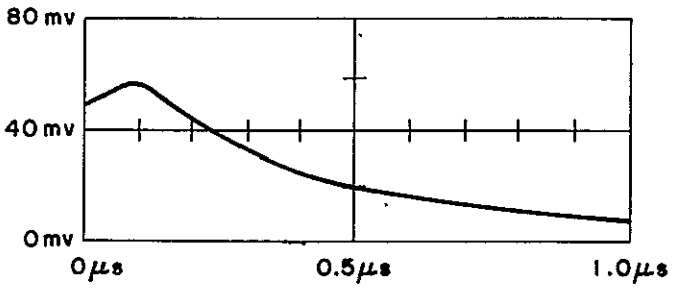

Figure 3.14 Photoconductive Decay for Cell #1135-2. E = 6 volts

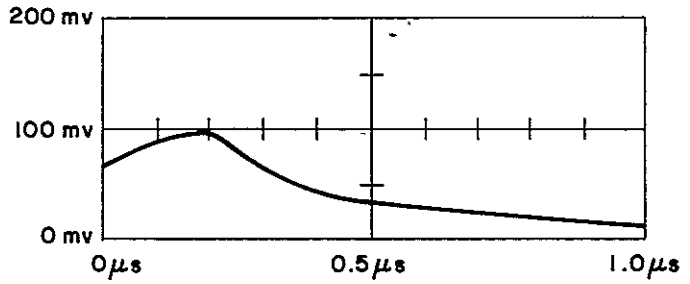

Figure 3.15 Photoconductive Decay for Cell #1135-2. E = 12 volts

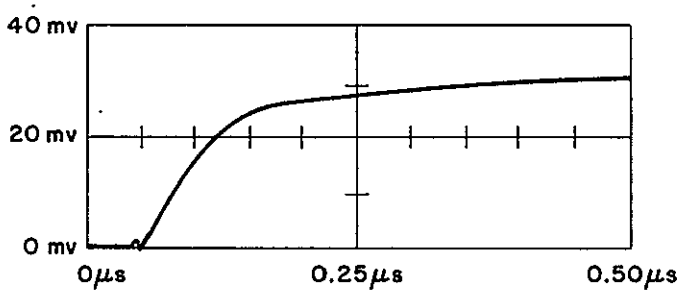

Figure 3.16 Photoconductive Rise for Cell #1135-2. E = 22.5 volts

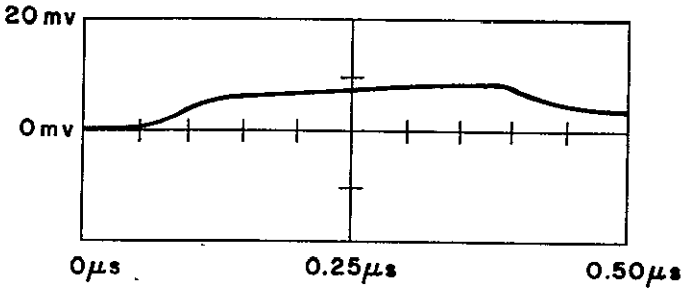

Figure 3.17 Photoconductive Rise and Decay of Cell #1135-1. E = 12 volts

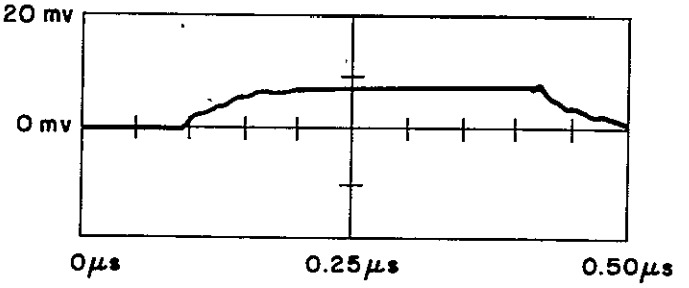

Figure 3.18 Photoconductive Rise and Decay of Cell #1135-1. E = 45 volts

4. NOISE AND D*

4.1 Noise

4.1.1 General

The main types of noise in photoconductors are current noise, generation-recombination noise, Johnson noise, and photon noise from surroundings. Only current noise and Johnson noise have been found in these detectors. Current noise is a general phenomenon in solid state devices but it is not well understood. However, when photoconductive detectors are operated with a matched load the noise voltage per root cycle follows the general form

$$Vn = \frac{B E f^{-a}}{\sqrt{\ell w d}} \tag{4.1}$$

where

B = constant

f = frequency

a = constant which is usually near 1/2.

E, ℓ, w, and d are as defined previously.

Note that the noise power has approximately a 1/f dependance and the term 1/f noise is often used.

If the impedance of the detector and measuring circuit is purely real, the Johnson noise voltage per root cycle with matched loads is

$$Vn = \sqrt{4kT}\sqrt{\frac{Ro}{2}} \tag{4.2}$$

Calculated values for these detectors are shown in Table 4.1.

4.1.2 Noise Measurements

The noise was measured using the same equipment used for measuring responsivity except that the cells were in the dark. An output from the wave analyzer was averaged with a 10 second RC network and displayed on an oscilloscope, and further averaged by eye for

about a minute. Readings were taken at bias voltage up to 45 volts and frequencies from 620 Hz to 50 KHz. The results for three of the detectors are shown in Figures 4.1, 4.2, and 4.3.

In general, the noise has a 1/f component which dominates at high fields and low frequencies. The frequency dependence has an increasingly negative slope as the bias is increased. Values of the slope, a, are shown in Table 4.2 as a function of bias, where it is seen that a approaches 1/2. The dependence on bias at 10 KHz is shown in Figure 4.4. It becomes linear as the 1/f noise predominates. The sub-linear result for 45 volts bias on two of the cells is not understood, but it is probably related to the reduction in signal discussed in section 3.3. The coefficient, B, has been computed for the four cells for which 22.5 volts bias is in the region where 1/f noise predominates. The results are shown in Table 4.3. The values of B are within an order of magnitude. Variations may be due to the uncertainty in the effective thickness and variations in silicon material.

4.2 D*

4.2.1 General

The two most common figures of merit for photodetectors are the Noise Equivalent Power (NEP) and the Detectivity (D*). The NEP is the number of watts on a detector which would yield a signal to noise ratio of one. D* is a somewhat artificial number which is the square root of the area divided by the NEP.

The measurement conditions for NEP and D* are specified by

1) the radiation source in terms of a black body temperature or the wavelength if a monochromatic source is used, as we have in this project,

2) the frequency of the assumed sinusoidally modulated radiation,

3) the bandwidth of the amplifier. In this report the usual case of normalization to a 1 Hz bandwidth is used. Otherwise, one must integrate the noise power over the bandwidth. These conditions are specified in the above order in a parenthesis following the figure of merit.

With the notations for signal and noise used above the relevant definitions for NEP and D* become:

$$NEP \equiv \frac{Vn}{\mathcal{R}} = \frac{Vn}{So}\,\frac{A}{Ho} \quad \text{watts/Hz}^{1/2} \tag{4.3}$$

$$D^* \equiv \frac{\sqrt{A}}{NEP} = \frac{So\ Ho}{Vn\ \sqrt{A}} \quad \text{cm - Hz}^{1/2}\text{/watt} \tag{4.4}$$

For both Johnson noise and 1/f noise limited detectors the NEP can be decreased without limit by decreasing the size of the detector. Since Johnson noise is independent of bias, and if the signal and 1/f noise increase linearly with bias, the maximum signal-to-noise (S_o/V_n) is obtained when the detector is operated in the 1/f noise region. In this case, using Equations 2.31, 3.2 and 4.1 in Equation 4.4, an expression for 1/f noise limited D* is obtained:

$$D^*(0.9\mu, f, 1) = \frac{FMK\tau}{Bn_o\sqrt{d}} \frac{f^a}{\left(1+(2\pi f\tau)^2\right)^{1/2}} \tag{4.5}$$

Thus D* is independent of area. The utility of such a figure of merit comes about when optical limitations exist.

One should also note that there is an optimum modulation frequency. If a = 1/2, then D* is a maximum when $f = (2\pi\tau)^{-1}$, and Eq. 4.5 becomes

$$D^*(0.9\mu, (2\pi\tau)^{-1}, 1) = \frac{FMK}{Bn_o\sqrt{d}} \sqrt{\frac{\tau}{4\pi}} \tag{4.6}$$

Thus, D* (maximum) is reduced only as $\sqrt{\tau}$ and not as τ. In other words, a faster detector is less sensitive but the signal-to-noise for the 1/f limited case is not reduced as strongly as the signal.

4.2.2 D*(0.9μ, f, 1) for Selected Cases

Using the results of section 3.3 for $\mathcal{R}$ and section 4.1 for V_n, D* (0.9μ, f, 1) can be computed. It is necessary to assume that Eq. 2.31, the response to sinusoidal inputs, is valid. The noise at frequencies greater than 50 KHz was assumed to follow the extrapolated curves in Figs. 4.1 through 4.3. The results for cell numbers 1135-1 and 1135-2 are shown in Fig. 4.5.

The peak D* occurs at 2 MHz for both. For sample 1135-1, it is 4.5×10^{10} cm-$Hz^{1/2}$/watt with an NEP of 9×10^{-13} watts/$Hz^{1/2}$. Cell 1135-2 had a maximum D* of 5×10^{10} cm-$Hz^{1/2}$/watt and an NEP of 6.8×10^{-11} watts/$Hz^{1/2}$.

TABLE 4.1

JOHNSON NOISE LIMIT WITH MATCHED LOADS ($R_L = R_o$)

cell #	R_o (K ohms)	Noise/root-cycle (nanovolts)
1114-1	360	54.2
1135-1	110	30.0
1041-1	35	16.9
1120-1	3.7	5.5
1135-2	11	9.5

TABLE 4.2

SLOPE OF 1/f NOISE, a, AS A FUNCTION OF BIAS: MATCHED LOAD CONDITIONS

cell #	Bias, E					
	1.5 v	3 v	6 v	12 v	22.5 v	45 v
1114-1	-	-	-	-	.15	.23
1135-1	.12	.14	.17	.36	.46	.41
1041-1	.16	.19	.32	.33	.38	-
1120-1	-	.15	.19	.27	.29	-
1135-2	.29	.34	.37	.32	.41	.40

TABLE 4.3

NOISE COEFFICIENT, B, AT 10 KHz AND 22.5 v BIAS

cell #	B
1135-1	1.3×10^{-7}
1041-1	6.7×10^{-7}
1120-1	1.3×10^{-7}
1135-2	3.5×10^{-7}

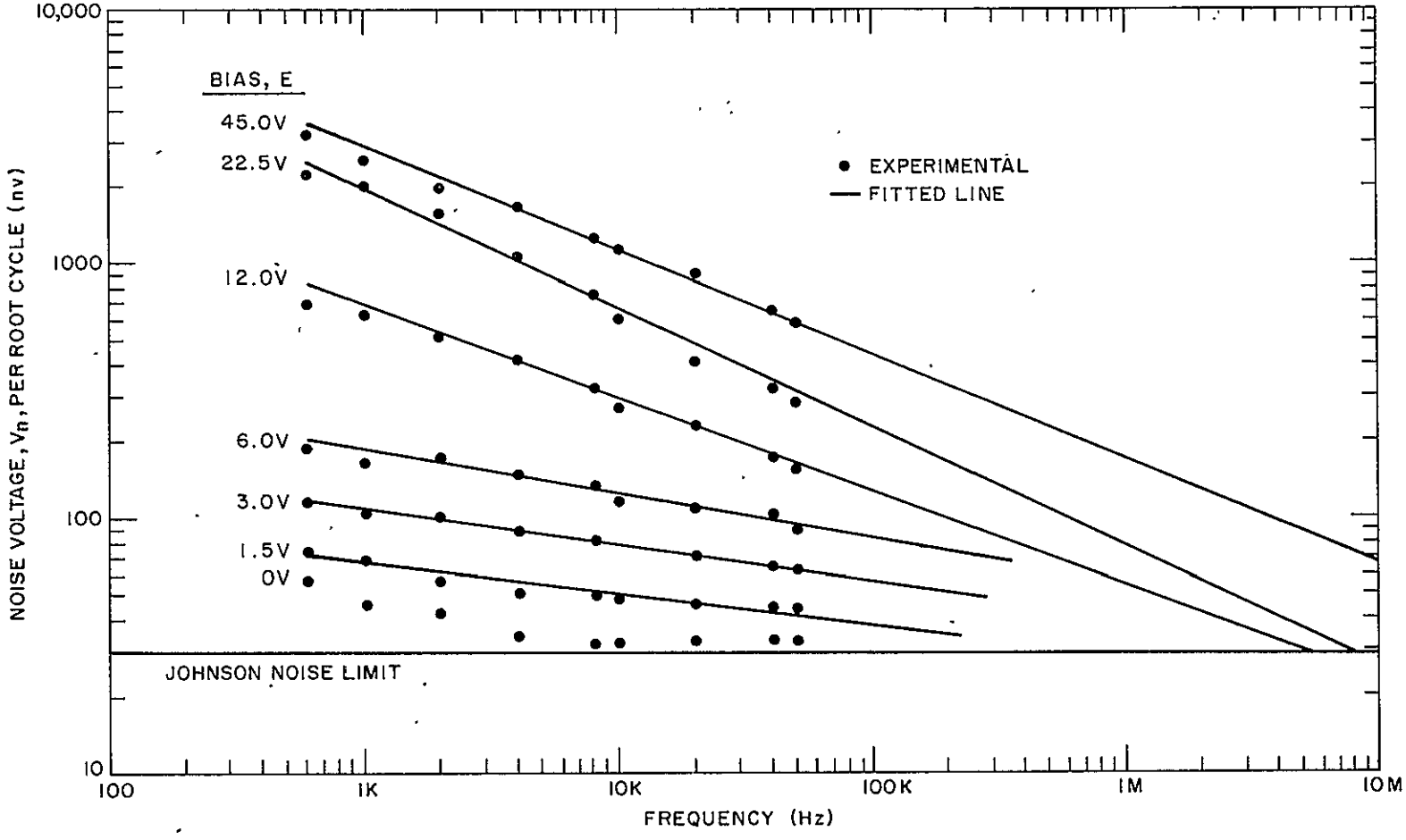

Figure 4.1 Noise Spectrum of Cell #1135-1

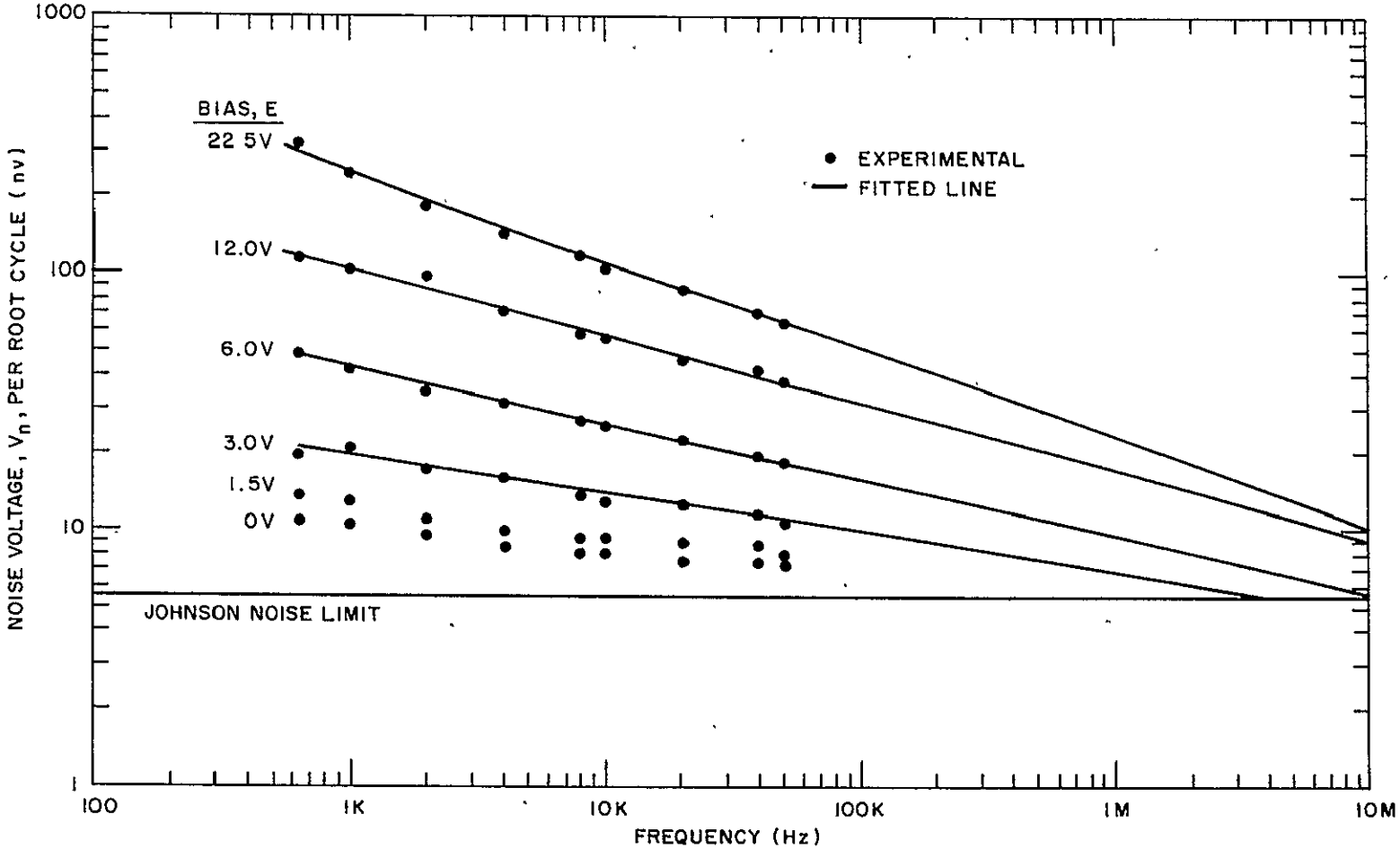

Figure 4.2 Noise Spectrum of Cell #1120-2

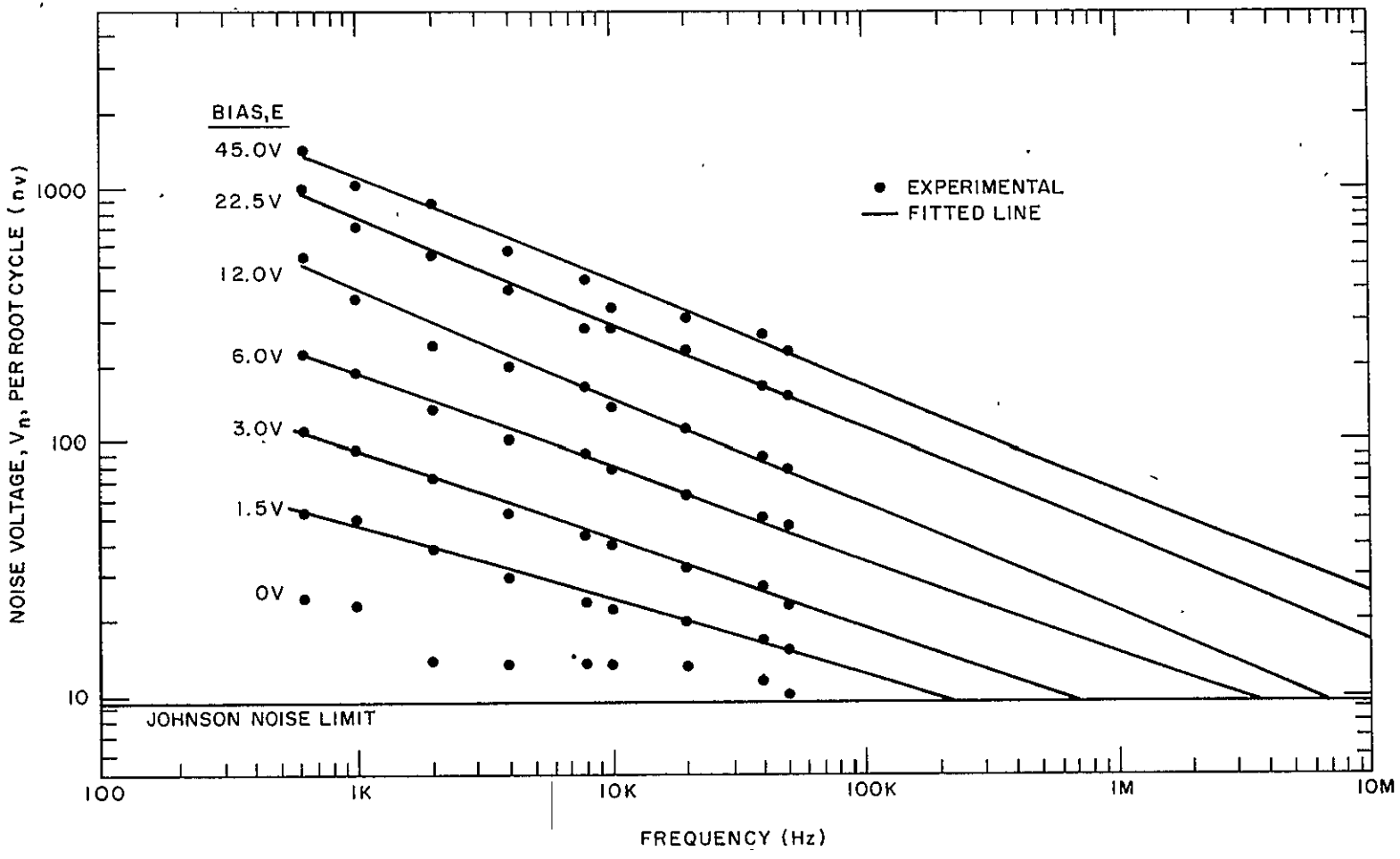

Figure 4.3 Noise Spectrum of Cell #1135-2

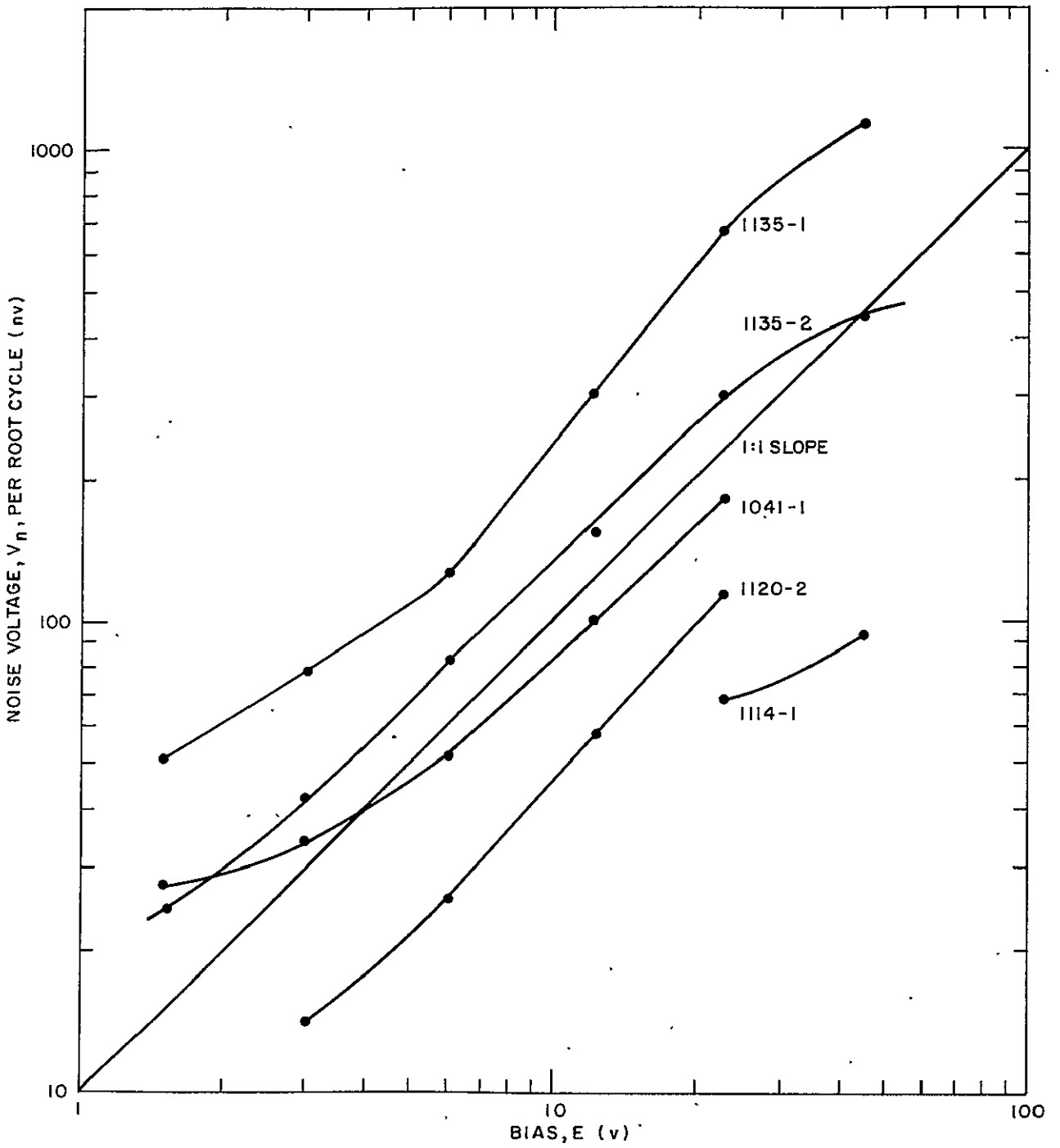

Figure 4.4 Noise Voltage, V_n, per Root Cycle vs. Bias, E, at 10 KHz

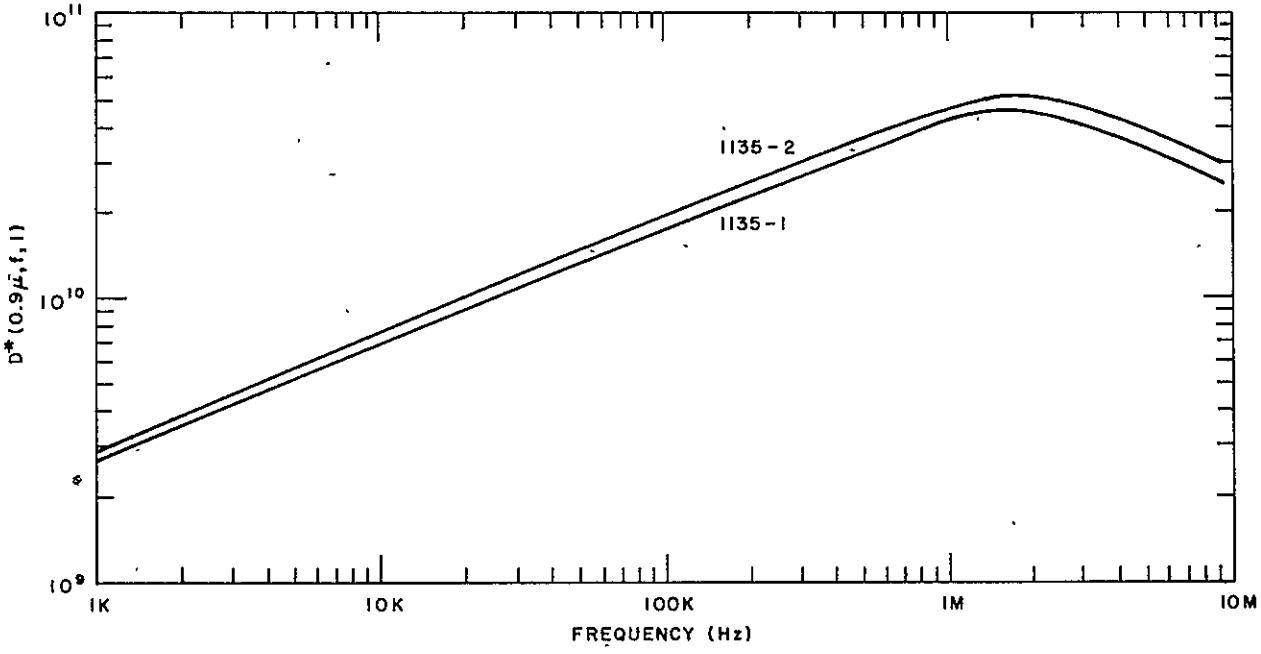

Figure 4.5 D* (0.9 μ, f, 1) for Cells #1135-1 and #1135-2 at a Bias of 45 volts

5. CONCLUSIONS AND SUGGESTIONS FOR FUTURE WORK

5.1 Conclusions

In the foregoing we developed a relatively simple model for the response of a PC detector by making the following assumptions:

1) only majority carriers need be considered

2) there are no traps present

3) the relaxation of the photo-generated carriers is described by a single exponential time constant

4) the surface recombination and the bulk mobility can be used to characterize an assumed homogenous material

5) diffusion can be ignored

6) the absorption coefficient is large

7) field inhomogenieties can be ignored and an effective thickness found.

With the above assumptions, the only measurements needed to predict the responsivity are the resistance to determine $1/n_o d$ and the recombination time, τ. All other factors are properties of a general nature for silicon. The results agreed reasonably well but become more uncertain as the extreme cases of very non-uniform geometry and high fields are encountered. The noise was also found to follow a relatively simple dependence on bias, frequency, and dimensions.

We should point out that the reduction of recombination time to less than 100 nanoseconds represents an improvement of two orders of magnitude for PC silicon detectors. This loses some of its significance because PV detectors can already operate in this frequency region. However, the D* and NEP of sample #1135-1 at 2 MHz are equal to or better than currently obtainable with PV detectors. Moreover, there are possibilities for improvement as discussed in the next section.

5.2 Suggestions for Future Work

It is obvious that a great deal of work can be done to reduce the number of assumptions in a more comprehensive model than the one presented in this report. However, Equation 3.2 for responsivity and Equation 4.6 for D* have an approximate validity which makes them useful for a discussion of the prospects for improvement.

Considering the factors involved in the expression for D*, we see that a 25% improvement can be made by reducing the reflection losses to zero. M has a maximum value of 0.25, but in cases where external capacitance is a problem, low impedance detectors are required. Thus practical methods of achieving low impedance configurations would be useful. The development of ohmic transparent electrodes would help here.

Since these detectors are 1/f noise limited, reduction of the noise coefficient, B, is worthwhile. At this time the practical limit to such reduction is not known. Reduction in n_o is probably possible since, although the nominal purity is within an order of magnitude of intrinsic, n_o is probably increased by surface impurities. Ultra clean surfaces would not only decrease n_o but would increase the recombination time yielding higher D*'s at lower frequencies.

For high frequency operation, the field dependent recombination time should be explored further. If it is due to recombination at an electrode, then the use of transparent electrodes on thin samples would yield nanosecond response times. If it is due to increased surface recombination, then the incorporation of neutral recombination centers is a possible method of improvement.

Lastly, a practical method for making ultra thin samples should be devised. The term $(1 - \exp(-\alpha d))/d$ appraoches α as d becomes small indicating that there is a limit to the improvement obtained. However, the absorption coefficient increases very rapidly at shorter wavelengths so that a large increase can be obtained in this region of the spectrum.

APPENDIX: PHOTOVOLTAIC JUNCTION DETECTORS

In this section we will briefly describe the PV type detector. The reason for doing so is the similarity to PC detectors in the form of the output signal and the fact that until recently these were the only type of silicon detectors commonly manufactured.

The device is a PN junction or diode with one side of the junction exposed to the illumination. When photons of the appropriate wavelength are absorbed the internal fields cause current to flow through an external load resistor. This current source is linearly related to the intensity and does not require an external biasing potential. The rise and fall times associated with the current source response are on the order of 10 nanoseconds.

A complete analysis of the operation in a circuit would yield equations similar to Equations 2.23 and 2.24 with $\tau = 10$ nsec. It would be more complicated since the rise and decay are not simple exponentials. However, an equation for the voltage signal on a load resistor due to a square light pulse is easily derived if we make the following assumptions:

1. The time scale of interest is large enough so that the current source rise and decay can be neglected.

2. The load resistor is much larger than the series resistance of the device (usually on the order of 100 ohms) and much smaller than the junction resistance (usually on the order of 100 megohms).

3. The output voltage is less than about $KT/q = 25$ mv. (If not, the output signal becomes a logarithmic function of light intensity.)

Under the above conditions, the voltage signal, S, obtained with a square light pulse of H_o watts/cm^2 will be

$$S(t < T) = S_o \left(1 - e^{-t/\tau_e}\right) \tag{1}$$

where now

$$S_o = \frac{FK \eta \tau_e}{C_o + C_L} H_o A \tag{2}$$

and

$$\tau e = R_L (C_o + C_L) \tag{3}$$

with the usual definitions of the other parameters. This is the same form as Equation 2.27 for recombination limited response in PC detectors. For PV detectors it is a non-trivial constraint since, even if $C_L = O$, the junction capacitance, C_o, may be as high as 1000 pf./cm^2 of active area. To reduce C_o a reverse bias is used on the junction, which reduces the capacitance inversely as the square root of the bias. An order of magnitude reduction can be obtained in this way, limited by reverse breakdown. (This is often called the photoconductive mode although it is not a photoconductive process.)

The PV detectors are specified in terms of amps/watt instead of volts/watt. The reason is clear if we rewrite Equation 1 as

$$S(t < T) = I_o R_L \left(1 - e^{-t/\tau e}\right) \tag{4}$$

where

$$I_o = FK\beta H_o A \tag{5}$$

At 0.9 microns, assuming F = 0.8, $I_o/H_oA = 0.58$ amps/watt. Typical values are in the range, 0.2 to 0.5 amps/watt.

With a specification of capacitance and sensitivity in amps/watt, one can compare PV versus PC signal and frequency response using the above equations subject to the constraints listed. For very high or very low frequencies, more information about the device would be needed.

It is also possible to find a short circuit current sensitivity for PC detectors. We note from Equation 2.19 that as R_L approaches O, $M(R_L/R_o)$ approaches R_L/R_o. Using the form of Equation 2.22, the short circuit signal, S_{sc}, becomes $4(R_L/R_o) S_o$ where S_o is the matched load signal. Assuming a real load impedance,

$$\frac{I_{sc}}{H_o A} = \frac{1}{R_L} \quad \frac{S_{sc}}{H_o A} = 4 \frac{R}{R_o} \tag{6}$$

There is no particular limit for this; values for the detectors in this report range from 0.25 to 8.0 amps/watt.

The major noise mechanisms for PV detectors are 1/f noise at very low frequencies (less than about 1 KHz), shot noise at intermediate frequencies, and Johnson noise at high frequencies. The dependence on load impedance, reverse bias, and frequency is too complicated for a simple exposition.

Unclassified

Security Classification

DOCUMENT CONTROL DATA - R&D

(Security classification of title, body of abstract and indexing annotation must be entered when the overall report is classified)

1. ORIGINATING ACTIVITY (Corporate author)	2a REPORT SECURITY CLASSIFICATION
MITHRAS, Inc. 701 Concord Avenue Cambridge, Massachusetts 02138	Unclassified
	2b GROUP None

3 REPORT TITLE

FAST RESPONSE SILICON PHOTOCONDUCTIVE DETECTORS

4 DESCRIPTIVE NOTES (Type of report and inclusive dates)

FINAL REPORT — Period Covered: January 15, 1967 — June 15, 1967

5 AUTHOR(S) (Last name, first name, initial)

Douma, Mark

6 REPORT DATE	7a. TOTAL NO. OF PAGES	7b NO OF REFS
June 15, 1967	44	0

8a CONTRACT OR GRANT NO.	9a ORIGINATOR'S REPORT NUMBER(S)
NAS 12-523 b PROJECT NO	MC 67-264-R1
c d	9b. OTHER REPORT NO(S) (Any other numbers that may be assigned this report)

10 AVAILABILITY/LIMITATION NOTICES

Reproduction in whole or in part is permitted for any purpose of the United States Government.

11 SUPPLEMENTARY NOTES	12. SPONSORING MILITARY ACTIVITY
	National Aeronautics & Space Administration Electronics Research Center 575 Technology Sq., Cambridge, Mass. 02139

13. ABSTRACT

The response time of a silicon photoconductive detector in a circuit containing capacitance depends on the recombination time of the photo-generated carriers and the RC response time of the circuit. A linear model is developed which gives the response of the detector in the circuit to square light pulses of arbitrary duration. The model and the expected reduction in RC response time using low impedance detectors is verified experimentally. Results are used to determine the responsivity.

It is also found that the carrier recombination time in these detectors varies inversely with the field under high field conditions (greater than about 100 volts/cm). A minimum carrier response time of 30 nanoseconds is obtained.

Current noise and Johnson noise are the only noise sources found measurable. The detectivity as a function of light modulation frequency is computed for selected cases. A value of 5×10^{10} cm-cps$^{1/2}$/watt is found at 2 MHz.

DD FORM 1 JAN 64 1473

Unclassified

Security Classification

14 KEY WORDS	LINK A		LINK B		LINK C	
	ROLE	WT	ROLE	WT	ROLE	WT
Silicon Detectors Infrared Detectors Photoconductive Silicon Recombination Time in Silicon (Field Effects)						

INSTRUCTIONS

1. ORIGINATING ACTIVITY: Enter the name and address of the contractor, subcontractor, grantee, Department of Defense activity or other organization *(corporate author)* issuing the report.

2a. REPORT SECURITY CLASSIFICATION: Enter the overall security classification of the report. Indicate whether "Restricted Data" is included. Marking is to be in accordance with appropriate security regulations.

2b. GROUP: Automatic downgrading is specified in DoD Directive 5200.10 and Armed Forces Industrial Manual. Enter the group number. Also, when applicable, show that optional markings have been used for Group 3 and Group 4 as authorized.

3. REPORT TITLE: Enter the complete report title in all capital letters. Titles in all cases should be unclassified. If a meaningful title cannot be selected without classification, show title classification in all capitals in parenthesis immediately following the title.

4. DESCRIPTIVE NOTES: If appropriate, enter the type of report, e.g., interim, progress, summary, annual, or final. Give the inclusive dates when a specific reporting period is covered.

5. AUTHOR(S): Enter the name(s) of author(s) as shown on or in the report. Enter last name, first name, middle initial. If military, show rank and branch of service. The name of the principal author is an absolute minimum requirement.

6. REPORT DATE: Enter the date of the report as day, month, year, or month, year. If more than one date appears on the report, use date of publication.

7a. TOTAL NUMBER OF PAGES: The total page count should follow normal pagination procedures, i.e., enter the number of pages containing information.

7b. NUMBER OF REFERENCES: Enter the total number of references cited in the report.

8a. CONTRACT OR GRANT NUMBER: If appropriate, enter the applicable number of the contract or grant under which the report was written.

8b, 8c, & 8d. PROJECT NUMBER: Enter the appropriate military department identification, such as project number, subproject number, system numbers, task number, etc.

9a. ORIGINATOR'S REPORT NUMBER(S): Enter the official report number by which the document will be identified and controlled by the originating activity. This number must be unique to this report.

9b. OTHER REPORT NUMBER(S): If the report has been assigned any other report numbers *(either by the originator or by the sponsor)*, also enter this number(s).

10. AVAILABILITY/LIMITATION NOTICES: Enter any limitations on further dissemination of the report, other than those imposed by security classification, using standard statements such as:

(1) "Qualified requesters may obtain copies of this report from DDC."

(2) "Foreign announcement and dissemination of this report by DDC is not authorized."

(3) "U. S. Government agencies may obtain copies of this report directly from DDC. Other qualified DDC users shall request through

_____."

(4) "U. S. military agencies may obtain copies of this report directly from DDC. Other qualified users shall request through

_____."

(5) "All distribution of this report is controlled. Qualified DDC users shall request through

_____."

If the report has been furnished to the Office of Technical Services, Department of Commerce, for sale to the public, indicate this fact and enter the price, if known.

11. SUPPLEMENTARY NOTES: Use for additional explanatory notes.

12. SPONSORING MILITARY ACTIVITY: Enter the name of the departmental project office or laboratory sponsoring *(paying for)* the research and development. Include address.

13 ABSTRACT: Enter an abstract giving a brief and factual summary of the document indicative of the report, even though it may also appear elsewhere in the body of the technical report. If additional space is required, a continuation sheet shall be attached.

It is highly desirable that the abstract of classified reports be unclassified. Each paragraph of the abstract shall end with an indication of the military security classification of the information in the paragraph, represented as *(TS), (S), (C), or (U)*

There is no limitation on the length of the abstract. However, the suggested length is from 150 to 225 words.

14. KEY WORDS: Key words are technically meaningful terms or short phrases that characterize a report and may be used as index entries for cataloging the report. Key words must be selected so that no security classification is required. Identifiers, such as equipment model designation, trade name, military project code name, geographic location, may be used as key words but will be followed by an indication of technical context. The assignment of links, roles, and weights is optional.